Feasibility of a Stewart Platform with Fixed Actuators as a Platform for CABG Surgery Device

Zoran Lazarevic

Master's Thesis

Columbia University
Department of Bioengineering

BEST AVAILABLE COPY

TABLE OF CONTENTS

A. INTRODUCTION 4

A. 1. Current State of Research 5

A. 1. 1. Minimally Invasive Coronary Artery Bypass Surgery 5

A. 1. 2. Robot Assisted Surgery 6

A. 1. 3. Tracking 8

B. METHODS 11

B. 1. Proposed Mechanism 13

B. 2. Inverse and Forward Kinematics 15

B. 2. 1. Inverse Kinematics 17

B. 2. 2. Forward Kinematics 18

C. RESULTS 23

C. 1. Choosing Joints for a Stewart Platform with Fixed Actuators 23

C. 2. Choosing Manipulator Dimensions 24

C. 3. Effect of Finite Actuator Step Length on Positional Accuracy 27

C. 4. Practical Considerations 33

C. 4. 1. Actuators 33

C. 4. 2. Joints 34

D. VISION, CONTROL AND TOOLING SUBSYSTEMS 37

E. CONCLUSION 40

F. LITERATURE 41

G. Acknowledgments 45

LIST OF FIGURES

Figure 1. Stewart Platform description 11
Figure 2. Stewart Platform with fixed actuators (SPFA). 13
Figure 3. Stewart Platform coordinate systems 15
Figure 4. The base and the platform shapes 16
Figure 5. Inverse kinematics 17
Figure 6. Trajectory 25
Figure 7. Stewart Platform with fixed actuators relative to the heart 26
Figure 8. Dimension calculation of the Stewart Platform 26
Figure 9. Positional and rotational errors. 31
Figure 10. The CAD model of the Stewart Platform with Fixed Actuators 36

A. INTRODUCTION

The coronary artery bypass graft (CABG) surgery is a commonly performed procedure worldwide. A device that would enable surgeons to perform the operation on a beating heart would make this procedure less invasive, thus reducing the post-operative complications.

The occlusion of a coronary artery prevents perfusion of the heart tissue and it may result in necrosis of the tissue and an infarct with a severe and life threatening damage to the myocardium [April96]. The purpose of the CABG operation is to provide blood flow through the coronary circulation by attaching a blood vessel (graft) from some other part of the body to a coronary artery. The sewing of the bypass graft to the coronary arteries entails very little detrimental physiologic impact to the patient and could, if there were no other issues, be considered a minor procedure in terms of patient recovery [Treat97]. What makes the operation fairly invasive and detrimental to the patient in the short run is the need to open the chest cavity ("sternotomy") to obtain access to the heart and also to place the patient's entire circulation on a cardio-pulmonary bypass machine. Although the negative effects, such as the post-operative pain, of the sternotomy are real, they are greatly overshadowed by the negative effects of the cardiopulmonary bypass machine. Placing a patient on the bypass machine is quite destructive to the circulating blood elements such as red cells and platelets and produces profound and sometimes life-threatening post-operative complications including bleeding and cerebrovascular strokes [Treas97]. The reason for placing the patient on the bypass machine is to keep the heart still while the surgeon performs the sewing of the graft onto the coronary arteries that are fairly small and require optimum conditions to work on [Borst97]. Although cardiac surgeons are attempting to sew grafts onto the beating heart, this procedure is obviously difficult and is at the outer limits of human surgical skill.

Surgical operations on the beating heart would be much easier to perform if the surgeon had a steady view of the heart surface. A video camera can provide a stabilized image of the heart. The idea behind this CABG surgery device is to move the video camera in concert with the heart and provide the surgeon with a view free of cardiac motion. The camera and custom-designed surgical instruments are mounted on a robotic manipulator. The camera motion is controlled by a heart motion-tracking algorithm. This provides the surgeon with a stationary picture of the heart on the video camera's monitor. The surgeon can then control the surgical instruments telerobotically and perform the surgery more easily.

This thesis describes a manipulator which will be used to move the camera and the surgical tools with high velocities and high accuracy. A parallel link manipulator called the Stewart Platform is proposed because of its advantages over serial link manipulators. The sections that follow review the current state of the art, describe the proposed mechanism, analyze its kinematic properties, and discuss design tradeoffs in building the mechanism. Simulation results are also presented for a number of designs.

A. 1. Current State of Research

A. 1. 1. Minimally Invasive Coronary Artery Bypass Surgery

Minimally invasive coronary artery bypass (CABG) surgery is a relatively new technique with increasing numbers of operations performed every year. Research is directed towards operation on the beating heart without need for cardiopulmonary bypass and heart access through small incisions. Most minimally invasive CABG procedures are limited to the cases of a single-vessel disease. The heart can then be accessed through a minithoracotomy, allowing anastamosis of the left internal mammary artery (LIMA) to left anterior descending coronary artery (LAD) [Mishra97]. The heart surface is stabilized using commercially available systems, for example the Access Platform and Stabilizer (CardioThoracic Systems, Inc., Cupertino, CA) [Cremer97] or by a suction device the Octopus Tissue Stabilizer (Medtronic, Inc., Minneapolis, MN) [Mack97a]. The motion of

a marker on the unrestrained heart surface covers an area of 15mm x 15mm. If the Octopus device is used to restrain the movements of the heart then the marker displacement is reduced to about 1mm x 1mm [Borst97]. The animal trials of a totally endoscopic CABG (E-CABG) are performed, using a stereo camera to obtain a three-dimensional video image. The heart is stabilized and a three-dimensional video head-mounted display is used for visualization of the operative field [Mack97a]. According to Mack, the procedures can be made more user friendly by means of robotic virtual immobilization of the heart surface. A high-speed tele-operated surgical robot would be placed in the chest cavity through ports and sit there in a "cardiostationary orbit", tracking a fixed point on the heart while the surgeon would be viewing a "virtually immobile" surgical field. Alternatives to the visual imaging are laser speckle surface imaging, three-dimensional confocal laser microscopy and mechanical spectroscopic imaging. Utilizing some of these technologies, only the structures of interest could be imaged creating virtually bloodless field for the performance of the procedure.

A. 1. 2. Robot Assisted Surgery

Robots are widely used for orthopedic surgery and stereotactic neurosurgery. They offer high precision positioning of the surgical instruments and better stability of the bone machining tools. Some examples of such robots are given in [Troccaz97]. ROBODOC is an active six Degree-Of-Freedom (6-DOF) robotic system for femoral bone machining in hip surgery, and AESOP (Computer Motion Inc) is a SCARA robot for laparoscopy with six DOF. The AESOP system can be controlled by the surgeon's voice. Four of its six DOF are active and two passive, which gives it some safety features. Some of the robot assisted surgical tools are configured as synergistic devices and utilize the force feedback. These include the Passive Arm with Dynamic Constraints (PADyC, TIMC Laboratory) and the knee surgery Active Constraint ROBOT (ACROBOT, Imperial College of London). ACROBOT employs backdrivable motors so that both the user and the motors together actuate the tool. These areas were, until recently, dominated by serial link manipulators as it can be seen from other overviews of medical robots [Burdea96],

[Khoda96]. [Lavallee96] describes a system for stereotactic neurosurgery in clinical use since 1989. The system uses a robotic arm with 6-DOF with repeatability of ±0.2mm. Commercially available robots like PUMA-560 [Santos95] and IBM Scara 7565 [Rovetta96] are often used. All these systems tried to integrate visual imaging with the three-dimensional data obtained by CT or MRI, but the surgeon was responsible for the control of the robotic tool. [Taylor96] presents a telerobotic system for laparoscopic surgery with intelligent trajectory and motion control, where the surgeon just points to the structure of interest and an algorithm handles the trajectory generation.

Recently, Stewart Platform (SP) type manipulators have been used for robotic assisted surgery. Stewart Platform with Fixed Actuators has been designed for ophthalmic surgery by Grace [Grace93]. An SP manipulator is being tested for image guided orthopedic surgery. After the registration of the manipulator position, a tool is mounted on the manipulator platform and the bone is machined. The problem of small workspace of the parallel link mechanisms is solved by adding special adapters that can reach the region of interest while the robot is moving within its working envelope. The robot workspace is 65x65x65 mm^3 if the angle between the base and the platform is less than 15° and the robot maximal velocity is 10mm/s [Brandt97].

Tele-robotic systems have also been proposed to solve problems in micro-surgery and remote surgery. The idea of using robots in microsurgery is to scale down a surgeon's motion by a master-slave manipulator. A cable driven 6-DOF manipulator for microsurgery called RAMS has been developed at JPL [Schener95]. An experimental master-slave 6-DOF scaling teleoperation system has been developed at the University of British Columbia, Canada. The manipulator is positioned near the region of interest by a larger 6-DOF robot. Both master and slave are magnetically levitated manipulators, the motion of the master is scaled-down to smaller motions of the slave and the scaled-up force feedback is applied to the master, in proportion to the force sensed by the slave end-effector [Salcu97]. Mitsuishi et al. implemented a master-slave tele-robotic system for micro blood vessel suturing with two small robotic arms. The surgeon can see on a

monitor a magnified image from a small CCD microscope. The display monitor moves, tracking the motion of the operator's face while the CCD microscope rotates correspondingly about the focal point of the microscope. The operator controls two rotational-force-feedback-free master-slave manipulators (only translational forces feedback) [Mitsu97]. Tele-robotic principles are applied also at larger distances: a robot in Italy was remotely controlled by a surgeon in the United States performing an operation on a model with a pig's organs. The two laboratories 10,000 km far from each other were connected via a satellite link [Rovetta96].

A. 1. 3. Tracking

A series of robotic systems for neurosurgery have been developed as a result of the ET project. Through its ten-year development, the systems went through a number of modifications, most of which involved different devices for tracking the position of an object in three-dimensional space [Reinhardt96]. The system was used to superimpose coordinates of the surgical instrument with the three-dimensional images recorded by a CT, so that the surgeon could accurately operate the tissues in the brain not easily identified by a human. The first version of the system employed a mechanical digitizer to determine the tool position and achieved an accuracy of ±3mm. The next version used the same principle to resolve the tool position, but a heavier and more robust digitizer arm yielded an accuracy of ±2mm. In the next stage of the project, ultrasonic spatial localization device Sonic Digitizer GP8-3D (Science Accessories Corp., Stratford, Conn.) could determine the positions of ultrasound transmitters in space, sampling the distances between the transmitters at the rate of 24kHz. The surgical instrument was now hand held, with the transmitters attached to it. The accuracy of the system was ±1mm. Three CCD line-scan cameras manufactured by Pixsys Inc. (Boulder, CO) were used in the following version of the system to detect positions of LEDs with the measuring accuracy of ±1mm.

Tracking of an object can be performed using ultrasound. Several piezzo-electric transducers can be attached to the mobile object and to some known points in space. Ultrasonic systems determine the position of the object by measuring the distances between the transducers. These systems can acquire the distances very fast, but the computation of the object position is very time consuming. Sonometrics Inc. system has been used to determine the shape of the heart surface but the actual position computation is done off-line [Dickstein96]. In order to speed-up the position estimation, the transducers can be arranged on the vertices of a cube [Alusi97].

Another system, often used for tracking the spatial position, is Optotrak manufactured by Northern Digital, Inc. It is an optical system with active IR beacons that are flashing one at a time, while their position is sensed by three line-scan CCD cameras, with an absolute accuracy better than ±0.1mm [Cutting96], [Taylor94]. Instead of active IR beacons that are connected to the electronic device with wires, some optical tracking systems use passive markers illuminated by an IR source BrainLAB (BrainLAB GmbH, Germany, VISLAN (Guy's Hosp., London, U.K.). If the markers are to be occluded during the surgical procedure, an electromagnetic system can be used (Polhemus Inc, Ascension Technologies Inc.), but large errors can occur if a ferromagnetic material is brought near the measuring system.

Taylor implants three pins into the bone and uses an off-the-shelf video camera to determine the position of the bone. An object can be tracked using a video camera by detecting four co-planar markers on the object, utilizing the principles of uncalibrated stereo. Sometimes an object to be tracked does not have a planar surface that can be used to attach the markers, for example a human leg. Uenohara and Kanade attach several markers on the object surface, record the images of the moving object and then choose only four of those markers that appear to be closely co-planar. Later, they use these four markers for tracking the object in space [Uenoh95]. Marker detection is simplified if an image of the region of interest is analyzed and a histogram of the colors in the image is

created. [Wei97] describes color coding for tracking of laparoscopic instruments based on the green color that does not appear in a laparoscopic image.

B. METHODS

A platform manipulator for the CABG surgery device would have to be able to move actuated surgical instruments and a camera, fast and precise enough to follow the heart movements and conform to safety requirements at the same time. Requirements for the manipulator design are:

- 6 Degrees-of-Freedom (DOF)
- Working volume of 50x50x50 mm
- Submillimeter positioning accuracy
- High velocity and acceleration
- High stiffness to eliminate vibrations
- Should enable surgeon access to the patient
- Easy to remove

As a possible actuating system, three options are investigated: Cartesian gantry, robotic arm and Stewart Platform-type manipulator. The first option is Cartesian 3-DOF gantry device (X-Y-Z table) placed over the chest cavity. Attached to the end point would be a small 3-DOF wrist that would orient the surgeon's tools. While this is conceptually the simplest device, we believe it may be difficult to actuate it with the required accelerations needed to null out the motion of the heart. The second option is a more conventional robotic arm with 6-DOF. This could be placed over the chest cavity from a distance, and could be more massive and stable. However, the accuracy and actuation velocities for this approach may also be prohibitive. Robotic arms are widely used in stereotactic neurosurgery because of their large workspace, but they are actuated at very low speeds.

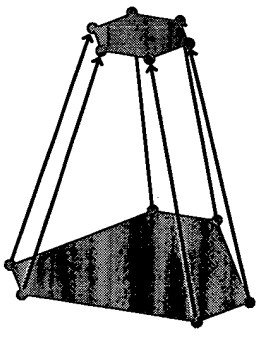

Figure 1. Stewart Platform consists of base, platform and six variable-length links that support the platform.

Although a gantry is conceptually the simplest device, a

Stewart Platform (which is referred to in the text that follows as an **SP**) is chosen because of its inherent advantages [Merletwww], [Fitcher86] over serial link manipulators, which are described below. It is configured as a platform connected to its base by 6 links whose length can change, offering controllability of 6 degrees of freedom. Being a parallel link manipulator, its positioning accuracy is better than the accuracy of individual actuators, the stiffness is high because forces are distributed to 6 links in the longitudinal direction and required actuating forces are small due to the light load. For instance, in serial link manipulators like a gantry or a robotic arm, the first motor has to support the weights of all the motors actuating the succeeding links. The drawbacks of the Stewart Platform-type manipulator are considerably smaller workspace and the existence of singular positions. The singular positions are the positions in which the mechanism cannot be controlled any more. An SP can reach these in many different ways, but there are apparently two different types of singularities. One appears when the platform gets into the same plane with one of the links. Another occurs when the platform rotates 90° about an axis perpendicular to it [Fitcher86].

B. 1. Proposed Mechanism

Stewart Platforms (**SP**) are commonly used in flight simulators and for positioning heavy tools, for instance in orthopedic surgery [Brandt97]. Extendible links are implemented there as hydraulic pistons, giving very high forces and stiffness but low velocities. Several other configurations are used in order to achieve larger workspace or higher speeds. In order to achieve higher speeds, a mechanism called a Stewart Platform with Fixed Actuators (which is referred to in the text that follows as an **SPFA)** is proposed. An **SPFA** has linear actuators fixed on the base moving links of constant length. The advantage of this approach is that power is not used to move heavy actuators but only lightweight links, and the actuators can be firmly fixed to the base to dampen high acceleration movements. The drawback is a smaller workspace in comparison with a standard **SP**, for the same travel of the linear actuators. Also, forces acting on the actuator have a perpendicular component, whereas forces exerted upon standard **SP** actuators have only a longitudinal component.

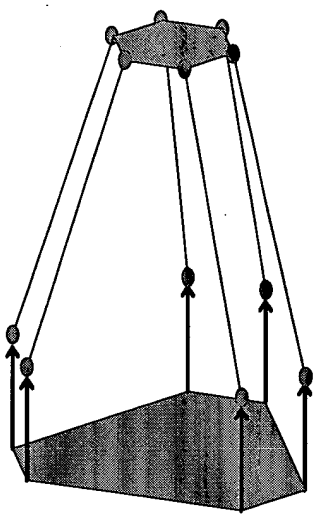

Figure 2. Stewart Platform with fixed actuators (SPFA). Actuators move in vertical direction acting on links.

Linear motion of the required velocity and acceleration can be achieved either by using linear electromotors or rotary electromotors with a converter from rotary to translatory motion. **Rotary electromotors** are relatively cheap and readily available, but their disadvantages are low transmission efficiency (around 60%) and mechanism inaccuracies introduced with each new moving part. Conversion from rotary to translatory motion is usually performed by ball-screw transmission or rack-and-pinion transmission. The ball-screw has a useful safety feature that in the case of a power shutdown the mechanism will be held in place. The rack-and-pinion transmission has better efficiency and is better

suited for the high speeds required for this application. **Linear electric motors**, on the other hand, are fast and their energy is directly transformed into linear motion.

It is interesting to note that the actuators **need not act linearly**: movement of an actuator along any trajectory, an arc for instance, would make possible the same motion of the platform, although the closed form inverse kinematics would not be possible in general case.

B. 2. Inverse and Forward Kinematics

Positions of the base and the platform are uniquely defined by the coordinates of the six joints that connect them with links. The six points are usually chosen to form an irregular hexagon in one plane, although, in general, they can be anywhere in the space. Vertices of the platform are defined by six vectors relative to the platform coordinate system {**P**}, and the base is defined relative to the base coordinate system {**B**}. Using homogeneous coordinates, the vector ${}^{P}\mathbf{p}_i=(px_i,py_i,pz_i,1)^T$ describes the position of the joint connecting the platform to the i-th link, with respect to {**P**}. Vector ${}^{B}\mathbf{b}_i=(bx_i,by_i,bz_i,1)^T$, describes the position of the i-th actuator.

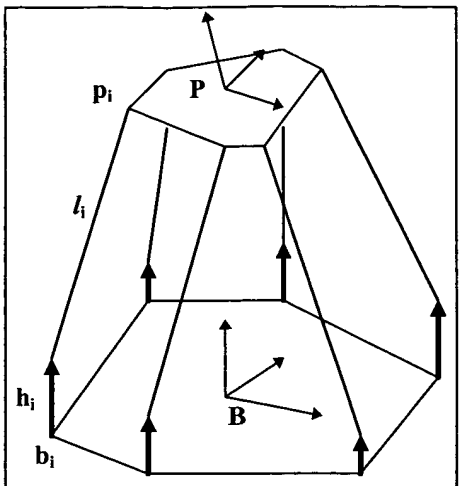

Figure 3. Stewart Platform with base coordinate system (**B**) and platform coordinate system (**P**)

The platform is supported by links of constant length $\mathbf{l}_i$, and the links attached to the actuators that can change the height $\mathbf{h}_i$, as shown in Figure 3.

The base is considered to be stationary, and a transformation is needed to find coordinates of the platform with respect to base coordinate system:

$$ {}^{B}\mathbf{p}_i = \mathbf{R}\ {}^{P}\mathbf{p}_i \qquad (1) $$

where **R** is a 4x4 homogeneous transformation matrix:

$$ \mathbf{R} = \begin{bmatrix} \mathbf{Rot}_{3x3} & \mathbf{T}_{3x1} \\ 0_{1x3} & 1 \end{bmatrix} \qquad (2) $$

where **Rot** denotes a rotation matrix and **T** a translation vector. The convention in this text is such that if no referent system is specified, the default is the base coordinate system.

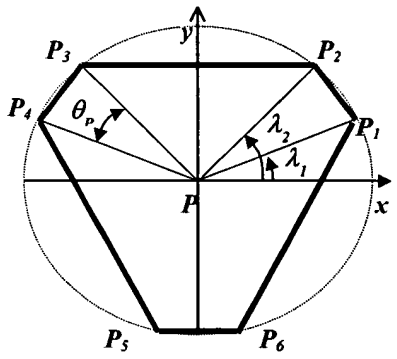

Figure 4. The base and the platform are usually designed as an irregular hexagon, whose shape is determined by an angle θ.

The base and the platform are usually designed as an irregular hexagon positioned in the x-y plane and symmetric with respect to the y-axis as in the Figure 4. The distance from the platform coordinate center to each platform joint ($\mathbf{P_1}$ - $\mathbf{P_6}$) is equal to the radius of the platform $\mathbf{r_P}$, and the shape is determined by an angle θ_P, between the first two joints. Similarly, the shape of the base and the coordinates of base joints ($\mathbf{B_1}$ - $\mathbf{B_6}$) are determined by $\mathbf{r_B}$ and θ_B. Now, denoting the angle between PP_i and x axis by λ_i (see Figure 4), and between BB_i and x axis by Λ_i for i=1,2,...,6 , we obtain:

$$\Lambda_i = 60^o \cdot i - \frac{\vartheta_B}{2}; \qquad \lambda_i = 60^o \cdot i - \frac{\vartheta_P}{2} \qquad \text{for i} = 1,3,5 \tag{3}$$

$$\Lambda_i = 60^o \cdot i + \frac{\vartheta_B}{2}; \qquad \lambda_i = 60^o \cdot i + \frac{\vartheta_P}{2} \qquad \text{for i} = 2,4,6 \tag{4}$$

As defined before, vector ${}^{P}\mathbf{p_i}=(px_i,py_i,pz_i,1)^T$ describes the position of the i-th platform joint with respect to platform coordinate system and ${}^{B}\mathbf{b_i}=(bx_i,by_i,bz_i,1)^T$ describes the position of the i-th base joint with respect to the base coordinate system. They can be written as:

$${}^{P}\mathbf{p}_i = \begin{bmatrix} r_P \cos\lambda_i & r_P \sin\lambda_i & 0 & 1 \end{bmatrix}^T \tag{5}$$

$${}^{B}\mathbf{b}_i = \begin{bmatrix} r_B \cos\Lambda_i & r_B \sin\Lambda_i & 0 & 1 \end{bmatrix}^T \tag{6}$$

for i=1,2,...,6.

Parallel and serial link manipulators have some dual properties: serial manipulators have high speed, large workspace, low precision and stiffness, whereas parallel manipulators have low speed, small workspace, high precision and stiffness. Their mathematics shows similar properties: it is straightforward to calculate forward kinematics of a serial link manipulator if all the joint positions are known, but inverse kinematics (find joint positions for known end-effector pose), in general, is obtained using iterative methods. Conversely, inverse kinematics calculation is straightforward for parallel link manipulators, when the end-effector position is given, and iterative methods are used for calculation of forward kinematics.

B. 2. 1. Inverse Kinematics

The inverse kinematics for **SPFA** can be formulated so as to determine required actuator heights for a given pose of the platform with respect to the base. Pose here implies both Cartesian position and orientation. **SPFA** actuators are considered to act linearly in the vertical direction, parallel to the z-axis, in order to simplify the mathematics, although that need not be the case. Actuator trajectory can be arbitrary, which can simplify the mechanics, but the closed form solution would not be possible, in the general case.

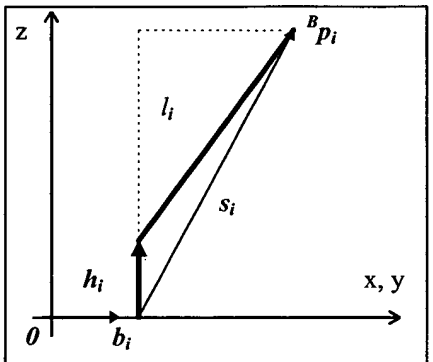

Figure 5. From the triangle, Pythagoras' theorem gives inverse kinematics for known $\mathbf{p_i}$ and $\mathbf{b_i}$

From the Figure 5, if the positions of the actuator position $\mathbf{b_i}$, platform joint $\mathbf{p_i}$ and the length of the link l_i are known, we have:

$$\mathbf{s_i} = \mathbf{p_i} - \mathbf{b_i} = \begin{bmatrix} x_i \\ y_i \\ z_i \\ 1 \end{bmatrix} \tag{7}$$

$$h_i = G(\mathbf{s_i}) = z_i - \sqrt{l_i^2 - (x_i^2 + y_i^2)} \tag{8}$$

This is a simple way to find the height of the i-th actuator. The solution is the point at the intersection of the actuator motion line and a sphere whose center is the platform joint $\mathbf{p}_i$ and with the radius equal to the link length $\mathbf{l}_i$ (Figure 5). Since there are two intersection points, the solution is not unique, and it even does not exist if the platform joint is too far from the actuator.

B. 2. 2. Forward Kinematics

The problem of forward kinematics is to determine the pose of the platform with respect to its base, given the actuator heights. The pose is defined by equation (1), as the dot product of the transformation matrix and the platform joint coordinates. The transformation matrix contains redundant information since its 4x4 elements can be uniquely found from six parameters that control six degrees of freedom. Here, we will choose these six parameters to be: x, y and z translation parameters and α, β and γ roll-pitch-yaw rotation parameters:

$$\mathbf{q}=[x \;\; y \;\; z \;\; \alpha \;\; \beta \;\; \gamma]^T \qquad (9)$$

Equations (7) and (8) define function (G:s→h), and since it cannot be inverted in a closed form, vector **s** can be estimated by linearizing function G(s(**q**)) around initial value of the actuator height h, with respect to vector **q**, using Newton's method. The following equations will consider only one actuator, so the subscript *i* will be left out for simplicity.

$$h = h_0 + \frac{dG}{d\mathbf{q}}\Delta\mathbf{q} \;\Rightarrow\; h - h_0 = \Delta h = \frac{dG}{d\mathbf{q}}\Delta\mathbf{q} \;\Rightarrow\; \Delta\mathbf{q} = \left(\frac{dG}{d\mathbf{q}}\right)^{-1}\Delta h \qquad (10)$$

$$\frac{dG}{d\mathbf{q}} = \frac{dG}{ds}\frac{ds}{d\mathbf{q}} = \frac{dG}{ds}\frac{d}{d\mathbf{q}}(\mathbf{R}(\mathbf{q})\mathbf{p}-\mathbf{b}) = \frac{dG}{ds}\frac{d\mathbf{R}}{d\mathbf{q}}\mathbf{p} \qquad (11)$$

From equation (8), we have a derivative of the function G with respect to s:

$$\frac{dG}{ds} = \begin{bmatrix} dG/dx \\ dG/dy \\ dG/dz \\ 1 \end{bmatrix} = \begin{bmatrix} 0 \\ 0 \\ 1 \\ 1 \end{bmatrix} + \frac{1}{\sqrt{l^2 - (x^2 + y^2)}} \begin{bmatrix} x \\ y \\ 0 \\ 1 \end{bmatrix} \qquad (12)$$

It is also necessary to determine $d\mathbf{R}/d\mathbf{q}$. Since $\mathbf{R}$ is a 2-dimensional matrix, and $\mathbf{q}$ is an 1-dimensional vector, the derivative will be 3-dimensional. It can be seen as six 4x4 matrices stacked together, the first one is the derivative of the transformation matrix with respect to the first element of vector $\mathbf{q}$, $d\mathbf{R}/d\mathbf{q}_1$, the second is $d\mathbf{R}/d\mathbf{q}_2$, and so on.

The elements of the transformation matrix depend on the translation and rotation. As previously stated, translation is determined by x, y and z values and rotation by roll-pitch-yaw angles α, β and γ. Pose of the platform coordinate system $\{\mathbf{P}\}$ can be obtained by the following sequence of fundamental rotations and translations of the base coordinate system $\{\mathbf{B}\}$:

1. First, rotate $\{\mathbf{B}\}$ about the $\mathbf{x_B}$-axis an angle γ(yaw).
2. Then rotate the resulting frame about $\mathbf{y_B}$-axis an angle β(pitch).
3. Rotate resulting frame about $\mathbf{z_B}$-axis an angle α(roll).
4. Translate the resulting frame by x, y and z along $\mathbf{x_B}$, $\mathbf{y_B}$ and $\mathbf{z_B}$ axes, respectively

The resulting homogeneous transformation matrix takes the following form:

$$\mathbf{R} = \begin{bmatrix} c\alpha \cdot c\beta & c\alpha \cdot s\beta \cdot s\gamma - s\alpha \cdot c\gamma & c\alpha \cdot s\beta \cdot c\gamma + s\alpha \cdot s\gamma & x \\ s\alpha \cdot c\beta & s\alpha \cdot s\beta \cdot s\gamma + c\alpha \cdot c\gamma & s\alpha \cdot s\beta \cdot c\gamma - c\alpha \cdot s\gamma & y \\ -s\beta & c\beta \cdot s\gamma & c\beta \cdot c\gamma & z \\ 0 & 0 & 0 & 1 \end{bmatrix} \qquad (13)$$

where $c\alpha = \cos\alpha$, $s\alpha = \sin\alpha$. Derivatives of the transformation matrix with respect to x, y, z, α, β and γ are given below:

$$\frac{d\mathbf{R}}{dx} = \begin{bmatrix} 0 & 0 & 0 & 1 \\ 0 & 0 & 0 & 0 \\ 0 & 0 & 0 & 0 \\ 0 & 0 & 0 & 0 \end{bmatrix} \tag{14}$$

$$\frac{d\mathbf{R}}{dy} = \begin{bmatrix} 0 & 0 & 0 & 0 \\ 0 & 0 & 0 & 1 \\ 0 & 0 & 0 & 0 \\ 0 & 0 & 0 & 0 \end{bmatrix} \tag{15}$$

$$\frac{d\mathbf{R}}{dz} = \begin{bmatrix} 0 & 0 & 0 & 0 \\ 0 & 0 & 0 & 0 \\ 0 & 0 & 0 & 1 \\ 0 & 0 & 0 & 0 \end{bmatrix} \tag{16}$$

$$\frac{d\mathbf{R}}{d\alpha} = \begin{bmatrix} -c\beta \cdot s\alpha & -c\gamma \cdot c\alpha - s\gamma \cdot s\beta \cdot s\alpha & c\alpha \cdot s\gamma - c\gamma \cdot s\beta \cdot s\alpha & 0 \\ c\beta \cdot c\alpha & c\alpha \cdot s\gamma \cdot s\beta + c\gamma \cdot s\alpha & c\gamma \cdot c\alpha \cdot s\beta + s\gamma \cdot s\alpha & 0 \\ 0 & 0 & 0 & 0 \\ 0 & 0 & 0 & 0 \end{bmatrix} \tag{17}$$

$$\frac{d\mathbf{R}}{d\beta} = \begin{bmatrix} -c\alpha \cdot s\beta & c\beta \cdot c\alpha \cdot s\gamma & c\gamma \cdot c\beta \cdot c\alpha & 0 \\ -s\beta \cdot c\alpha & c\beta \cdot s\gamma \cdot s\alpha & c\gamma \cdot c\beta \cdot s\alpha & 0 \\ -c\beta & -s\gamma \cdot s\beta & -c\gamma \cdot s\beta & 0 \\ 0 & 0 & 0 & 0 \end{bmatrix} \tag{18}$$

$$\frac{d\mathbf{R}}{d\gamma} = \begin{bmatrix} 0 & c\gamma \cdot c\alpha \cdot s\beta + s\gamma \cdot s\alpha & c\alpha \cdot s\gamma - c\gamma \cdot s\beta \cdot s\alpha & 0 \\ 0 & -c\alpha \cdot s\gamma + c\gamma \cdot s\beta \cdot s\alpha & -c\alpha \cdot c\gamma - s\gamma \cdot s\beta \cdot s\alpha & 0 \\ 0 & c\gamma \cdot c\beta & -s\gamma \cdot c\beta & 0 \\ 0 & 0 & 0 & 0 \end{bmatrix} \tag{19}$$

To summarize, matrix $\mathbf{H} = dG/d\mathbf{q}$ is a 6x6 matrix whose elements are:

$$\mathbf{H}_{i,j} = \frac{dG(\mathbf{s}_i)}{d\mathbf{q}_j} = \frac{dG(s_i)}{ds}\left(\frac{d\mathbf{R}}{d\mathbf{q}_j}\right)_{4x4}\left(\mathbf{p}_i\right)_{4x1} \tag{20}$$

Below is the algorithm for forward kinematics. It takes as input the model of the base **b** and the platform **p**, and the heights of the actuators $\mathbf{h}_0$. The output is the pose of the platform represented by the transformation matrix **R** or the pose vector **q**.

1. Select initial guess of the pose **q**
2. Compute transformation matrix **R=R(q)**, from (13)
3. Calculate **s = R p - b**
4. Use inverse kinematics to find actuator heights: **h**=G(**s**) according to (8)
5. Calculate height errors: $\Delta\mathbf{h} = \mathbf{h} - \mathbf{h}_0$
6. IF $|\Delta\mathbf{h}| < \varepsilon$ THEN STOP
7. Calculate matrix **H** from (20)
8. Solve $\Delta\mathbf{h}=\mathbf{H}\,\Delta\mathbf{q}$ for $\Delta\mathbf{q}$
9. Update platform pose, $\mathbf{q} = \mathbf{q} + \Delta\mathbf{q}$
10. GOTO step 2

The algorithm performs iterations, calculating the increment in the platform pose $\Delta\mathbf{q}$ and the link lengths for the new pose **h**. It terminates when the difference $\Delta\mathbf{h}$ between the calculated and the desired actuator positions drops below a small number ε.
Step 8 involves implicit inversion of matrix **H**. If the matrix is nearly singular, that means the position is close to the singular position and special attention is necessary.

Equation (10) gives the relationship between the infinitesimal changes of actuator heights and the changes in pose. Dividing both sides of that equation by an infinitesimal time period gives a relationship between actuator velocities and the platform translational and rotational velocities. The inverse of matrix **H** is also called the Jacobian matrix:

$$\mathbf{J} = \mathbf{H}^{-1} \qquad (21)$$

$$\dot{\mathbf{q}} = \mathbf{J} \cdot \dot{\mathbf{h}} \qquad (22)$$

This method is general in the sense that all the joints of the platform or actuators on the base need not be in one plane. This fact is useful if the joint coordinates are estimated after the manipulator is manufactured, and new, re-calibrated values are used for the forward kinematics.

It is important to note that the solution for forward kinematics is not unique. It is not necessary to have actuator height feedback if feature space feedback is used and approximate position of the actuators is known. However, if the manipulator enters singular position, platform pose cannot be calculated with confidence from actuator heights.

For the standard configuration of a Stewart Platform, faster methods for forward kinematics exist when joints are coplanar [McAcree96]. These methods involve inverting a 3x3 instead of a 6x6 matrix, so that they can be written in the closed form. I am not aware of such a method that can be applied to a Stewart Platform with Fixed Actuators.

C. RESULTS

C. 1. Choosing Joints for a Stewart Platform with Fixed Actuators

A Stewart Platform with Fixed Actuators (**SPFA**) has six degrees of freedom, which are controlled by changing the heights of six actuators. The mechanism should be designed so that the joints connecting actuators, links and a platform have enough freedom to achieve the desired motion. Also, when the actuators are fixed in one position, the mechanism should have zero Degrees-Of-Freedom (DOF), or in other words, the platform should be fixed in one position.

A general form of the DOF equation for both planar and spatial mechanism can be written as follows [Yang84]:

$$F = \lambda(l - j - 1) + \sum_{i=1}^{j} f_i - I_d \qquad (23)$$

where:

F = the effective DOF of the assembly or mechanism

λ = the DOF of the space in which the mechanism operates (for spatial motion $\lambda = 6$, and for motion in a plane or on a surface $\lambda = 3$)

l = number of links

j = number of joints

f_i = Degrees-Of-Freedom of i-th joint

I_d = idle or passive Degrees-Of-Freedom

There are special geometrical conditions that have to be taken into account in the determination of the DOF. For instance, one shaft with both ends fixed with ball joints has one idle DOF, and that is rotation about the axis that passes through both of the joints. The term I_d takes care of these cases. We are considering an **SPFA**, with n links, when all actuators are fixed. Referring to Figure 2, we have $\lambda = 6$ for spatial motion, $l = n + 1 + 1$

for six links, platform and base, $j = 2 \cdot n$ as the number of mobile joints in the mechanism. If the ball-and-socket joints are used, then $f_i = 3$, since every such a joint has three degrees of freedom. Each link connects rigidly two ball-and-socket joints, so that we have $I_d = n$ idle degrees of freedom. Equation (23) evaluates to:

$$F = 6\,(n+1+1 - 2n - 1) + 2n \cdot 3 - n = 6 - n \qquad (24)$$

Instead of ball-and-socket joints, universal joints can be used with an addition of a cylindrical joint positioned somewhere along the each link. Then we have $\lambda = 6$ for spatial motion, $l = n + 1 + 1 = 8$ for six links, platform and base, $j = 3 \cdot n$ as the number of mobile joints in the mechanism. There are twelve universal joints each having two degrees of freedom ($f_i = 2$, for $i=1,..,2n$) and six cylindrical joints each having one degree of freedom ($f_i = 1$, for $i= 2n+1,.., 3n$), and there are no idle degrees of freedom in the mechanism, $I_d = 0$. In this case, equation (23) gives:

$$F = 6\,(2n+1+1 - 3n - 1) + 2n \cdot 2 + n \cdot 1 = 6 - n \qquad (25)$$

Equations (24) and (25) show that the mechanism will be stiffly positioned if it has n=6 links, i.e. the Degrees-Of-Freedom of the platform will be zero.

C. 2. Choosing Manipulator Dimensions

Dimensions of the manipulator have to be chosen to satisfy several contradictory conditions:

- small overall size of the mechanism
- large base to provide stability
- small base to avoid singularities due to rotation about a horizontal axis
- short link lengths to provide stiffness and small positioning error
- large workspace requires long links

Dimensions are calculated taking as a main requirement, the anticipated trajectory of the manipulator. The tracking platform should follow a trajectory whose shape is close to a

circular arc of the radius **R** = 10 cm, maintaining constant distance and relative orientation with respect to the markers on the heart surface, as shown in Figure 6. The angle spanned by the trajectory is $\Phi = 90^{\circ}$,

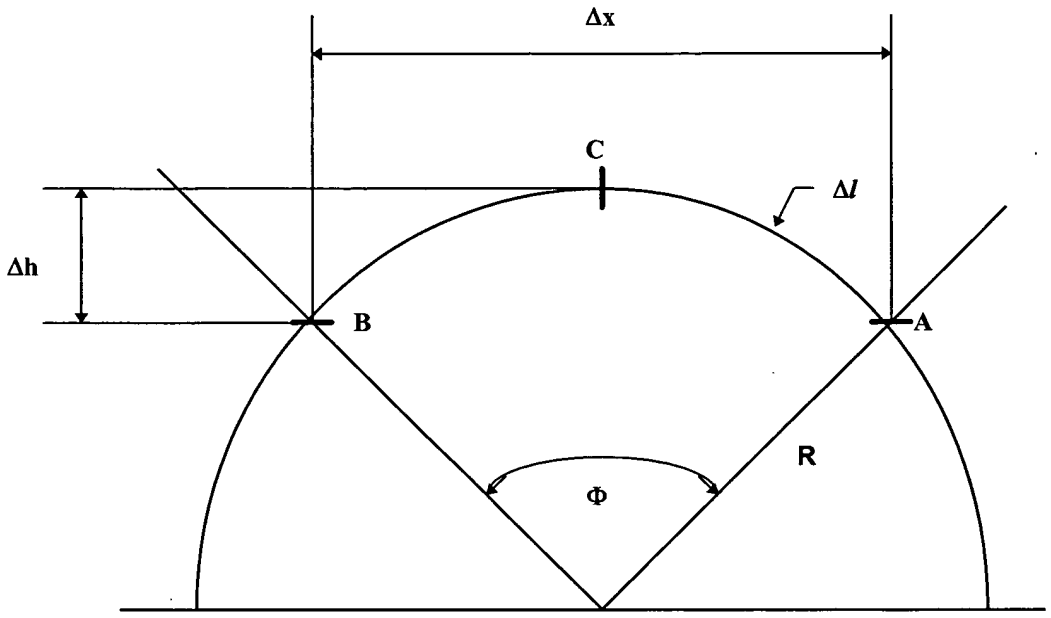

Figure 6. Trajectory is approximated with an arc from point A, through point C, to the point B.

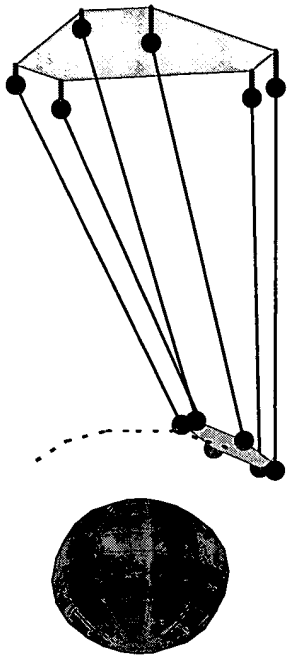

Figure 7. Stewart Platform with fixed actuators relative to the heart and platform trajectory marked with a dotted line,

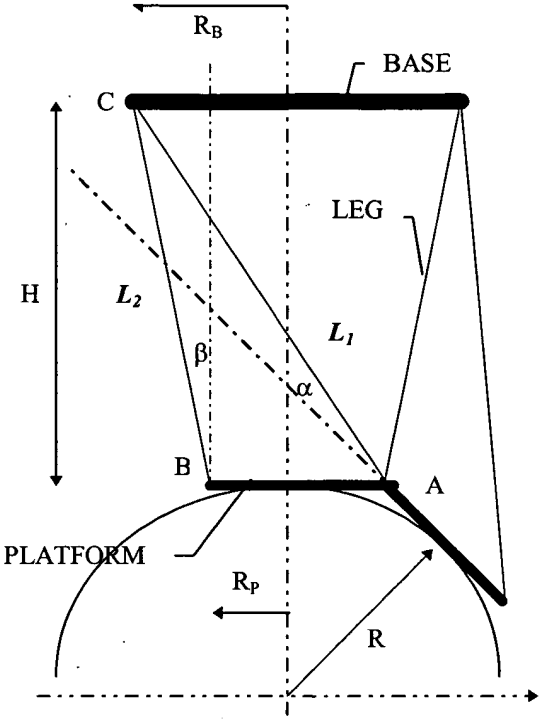

Figure 8. Approximate dimensions of the Stewart Platform can be calculated choosing margin angles α and β. Platform is observed in neutral position and at the end-point of the trajectory.

In order to avoid singularities, a security margin of 15° between the platform and the links is taken. The dimensions of the actuator are calculated from there using simple trigonometry. Figure 8 represents a simplified drawing of an **SP**. The platform is observed in two positions: in the "neutral" position at the lowest point of the trajectory (point denoted with B in Figure 8), and at the end-point of the trajectory (point A). At the point C, where lines $\mathbf{L_1}$ and $\mathbf{L_2}$ intersect, the lower joint of a link should be placed. Taking platform radius to be r_p= 3 cm, base radius and height of the platform in neutral position can be calculated. From these values it is easy to derive link lengths and obtain, through simulation, actual margin angles. Calculated parameters of the **SP** is given in the following table:

$\mathbf{r_b}$ = 7.6 cm	radius of the base
$\mathbf{r_p}$ = 3.0 cm	radius of the platform
H = 26.0 cm	height of the platform in neutral position

The manipulator with these dimensions looks tall and slender, with height to width ratio greater than 3:1. That means that oscillations might occur if the links are not rigid enough. The manipulator would be shorter and stiffer if the requirements for the platform rotation about the horizontal axis are weakened.

C. 3. Effect of Finite Actuator Step Length on Positional Accuracy

Due to the finite accuracy of the actuators, joint misplacement and other unmodelled effects, the actual platform position will differ from the commanded one. Closing a feedback loop in the control system decreases the systematic error due to differences between the ideal and the real model. Since the error due to the finite length of the actuator step cannot be eliminated, we need to investigate the effect of this finite length on the platform positional accuracy. To evaluate positional accuracy, we simulate an **SPFA** moving along a chosen trajectory and calculate maximal position errors and maximal orientation error. Sensitivity of the pose, meaning both position and orientation, is defined as the difference between commanded and achieved positions. Translation and rotation are treated differently because of the different nature of their contribution to the joint error.

The **position error** is distance of the center of the platform from the expected position. The **rotation error** is calculated in the following manner. A camera is positioned in the center of the platform. A point in the space is imaged by two cameras, one on the error-free platform, and one on the platform with errors. The error is calculated as the distance between the perspective projections of the point. The camera focal length is set to

$\mathbf{f} = 1$cm. The idea behind this way of measuring the error is that it includes both the position and the orientation error in the same quantitative value. The rotation error is also expressed in degrees, by calculating the angle between the platform normal in the desired and actual positions.

The algorithm used to calculate the error, given desired pose $\mathbf{R_D}$ and actuator step size Δh:

1. Calculate desired actuator heights $\mathbf{h_D}$ using inverse kinematics according to the equation (8)
2. Round the heights to the nearest multiple of Δh: $\mathbf{h_A} = \Delta h \cdot \lfloor \mathbf{h_D} / \Delta h + 0.5 \rfloor$
3. Use forward kinematics to find actual pose from $\mathbf{h_A}$ using $\mathbf{R_D}$ as initial guess

The shape of the base and platform is and the sensitivity is calculated for three configurations. The shapes of the base and the platform are chosen to vary from regular hexagon, through irregular hexagon to a triangle. Other parameters of the manipulator are as calculated before for the trajectory in Figure 6:

$\mathbf{r_b} = 7.6$ cm Radius of the base

$\mathbf{r_p} = 3.0$ cm radius of the platform

$\mathbf{H} = 26.0$ cm height of the platform in neutral position

The results for the **actuator step size of 0.1 mm** and for three different configurations of the manipulator, are given in the following table:

Dependence of the manipulator performance on the base and platform configuration	travel [cm]	speed [cm/rad]	min. link-platform angle[deg]	maximal position error [mm]	maximal rotation error[mm],[°]
Platform 1 hex base / hex platform θ_P=0° θ_B=30°	4.717	9.593	18.1	0.80	0.144 0.83°
Platform 2 hex base/ Δ platform θ_P=-60° θ_B=30°	6.099	10.615	16.8	0.24	0.047 0.27°
Platform 3 Δ base / Δ platform θ_P=-60° θ_B= 60°	6.800	11.126	15.5	0.15	0.037 0.21°

Travel is maximal displacement of the actuator needed to sweep the trajectory. **Speed** is expressed relative to the angular velocity of a point moving along the trajectory. **Minimal link-platform angle** represents the smallest of the angles between the six links and the platform plane, along the trajectory. In the simulation, the motion of the platform is such that it minimizes the rotation around the platform normal, and for that case, if the link and platform are in the same plane (i.e. link-platform is angle 0°) the manipulator will be in a singular position. In fact, the calculated minimum platform-link angle achieved in the simulation is close to the desired design parameter of 15°. Angles θ_P and θ_B determine the shape of the platform and the base, respectively, as shown in the Figure 4 on page 16. Further calculations have shown that the dependence of the positional and rotational error on the actuator step is approximately proportional. Hence, if the system with very accurate motors is developed, the required accuracy for the manipulator will be gained.

As we can see from the above table, when both base and platform are triangle shaped, the accuracy is the greatest, but the required travel of the actuator is the longest. Although a triangular base triangular platform yields the highest positional accuracy, it is unattainable in the real world since it requires that two actuators (which have finite size) be attached to the same point of the base. Configuration 2 (the semi-hexagonal base and triangular platform) is the best compromise since it allows real actuators of finite size to be placed

close together. On the other hand, double U-joints permit two vertices of the platform to be essentially at the same point [Fitcher86].

The above method of error measurement is somewhat random, because the maximal error in the simulation depends on the actuator step size and on the initial heights of the actuators. Another way of presenting accuracy of the Stewart Platform manipulator is to calculate the "average" error for a given pose. In the Figure 9 are shown the averaged positional and rotational errors. The manipulator with semi-hexagonal base and triangular platform is used for the calculation.

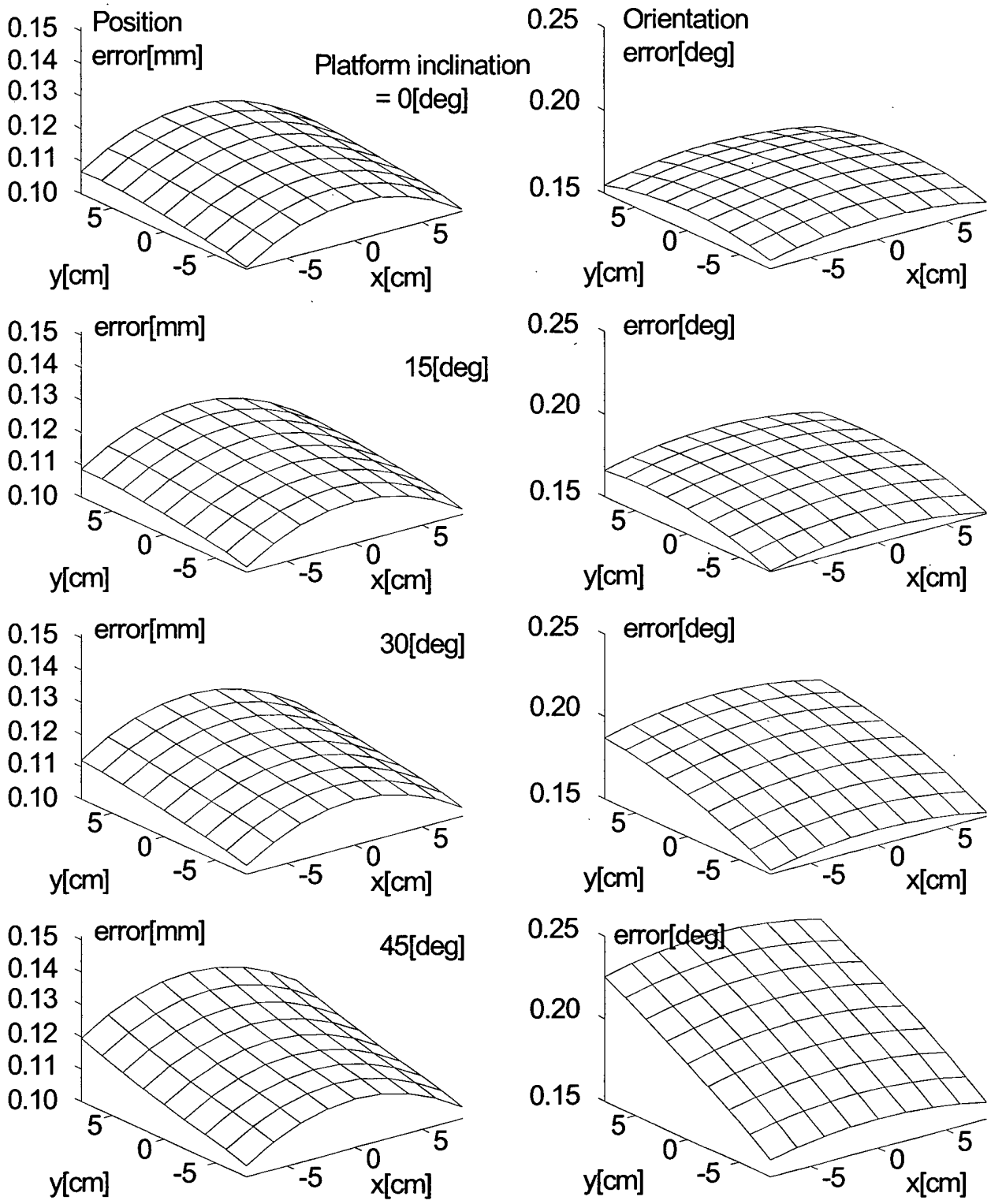

Figure 9. Positional (left) and rotational (right) errors when the platform moves along a sphere 10cm from the center of the heart. The graphs show errors for the inclination of the platform with respect to the base of 0°, 15°, 30° and 45° (top to bottom) . The actuator displacement is 0.1 mm.

The errors in position and orientation of the platform caused by an infinitesimal displacement of each link are calculated first, and then averaged in a certain way to give one value. The Jacobian tells us how much the platform will move if the actuators move by an infinitesimal amount:

$$\mathbf{J} = \frac{d\mathbf{q}}{d\mathbf{h}} \qquad (26)$$

The vector $\boldsymbol{h}$ has six elements, each element being the height of one actuator. The vector $\boldsymbol{q}$ has also six elements, tree determining rotation (q_x, q_y, q_z) and tree determining orientation (q_α, q_β, q_γ). The vector of the actuator height displacements $\Delta\boldsymbol{h}$ has six elements, each being the displacement of one actuator from its desired height. When the manipulator kinematics is linearized, the error due to the displacements of the actuator is:

$$\Delta\mathbf{q} = \mathbf{J} \cdot \Delta\mathbf{h} \qquad (27)$$

The error due to the displacement of the i-th link can be calculated from the previous equation, when all the elements of $\Delta\boldsymbol{h}$ are set to zero, except for the i-th, which is set to the displacement value Δh.

$$\Delta\mathbf{h} = \begin{bmatrix} 0 & 0 & \dots & 0 & \Delta h & 0 & 0 \end{bmatrix}^T \qquad (28)$$

The six error vectors are obtained from equation (27): $\Delta\boldsymbol{q}_1$, $\Delta\boldsymbol{q}_2$,..., $\Delta\boldsymbol{q}_6$. The positional errors are averaged by the following formula:

$$\mathbf{e}_{POS} = \sqrt{\frac{1}{6}\sum_{i=1}^{6}(\Delta q_{xi}{}^2 + \Delta q_{yi}{}^2 + \Delta q_{zi}{}^2)} \qquad (29)$$

and similarly, the orientation errors are averaged:

$$\mathbf{e}_{OR} = \sqrt{\frac{1}{6}\sum_{i=1}^{6}(\Delta q_{\alpha i}{}^2 + \Delta q_{\beta i}{}^2 + \Delta q_{\gamma i}{}^2)} \qquad (30)$$

The graphs show that the positional error does not change much when the platform is inclined with respect to the base, but the rotational error increases with the inclination angle.

C. 4. Practical Considerations

C. 4. 1. Actuators

The Stewart Platform with Fixed Actuators (SPFA) needs linear actuators. Linear motion can be obtained from linear electrical motors, or by converting rotary to linear motion. The low-end version of the manipulator would benefit from the rotary stepper motors, which are readily available, cheap and relatively easy to control using discrete steps. That also means that the manipulator can be actuated open loop, if the position of the actuator is estimated by a product of the number of motor steps and the step size. If a rotary motor is used as an actuator, some kind of transmission from rotary to linear motion is needed. Rotary motion is usually converted to linear movements using the rack-and-pinion or the ball-screw transmission.

The advantages of the rack-and-pinion over ball-screw transmission are:

- allows easy adjustment of the rotary-to-linear transformation constant by choosing different pinion radius
- takes less space in vertical direction because the motor can be placed perpendicular to the rack
- more appropriate for higher speeds, if the pinion radius is appropriately chosen
- better efficiency

The advantages of the ball-screw over the rack-and-pinion transmission are:

- zero backlash
- the platform stops in the case of power shutdown

Whether the linear or rotary motors are used, a spring is needed to oppose the gravity, since the actuators will be used in the vertical direction. The spring length should be at least three times the travel of the actuator, which would considerably increase the dimension of the device. This problem could probably be solved if the ball-screw mechanism is employed, but at the cost of having a slower and less efficient system.

The following calculations are performed to verify if the required velocities and accelerations could be achieved if some off-the-shelf rotary motors are used. The load of 2kg is supported by six links and the average load per link is taken to be one sixth of the mass, so $m = 1/6 \cdot 2kg = 0.33\ kg$. The travel of the actuators is $h = 5\ cm$, the root-mean-square speed of the linear actuator is $V_{rms} = 1\ m/s$, root-mean-square acceleration is $a_{rms} = 20m/s^2$ and the transmission efficiency of the rotary-to-linear conversion is $\eta = 60\%$. A DC servo motor AEROTECH Model 1050 has the rotor inertia $J_m = 5.7e\text{-}05\ kg\ m^2$. Then, the optimal radius of the rotary-to-linear conversion pinion would be

$$r_{opt} = sqrt(\eta \cdot J_m/m) = 1.0129\ cm$$

The radius is then chosen to have some standard value, $r = 0.5 \cdot 1" = 12.7\ mm$, which yields the root-mean-square angular velocity $\omega_{rms} = V_{rms}/r = 79\ rad/s = 752\ rpm$, and the root-mean-square angular acceleration $\alpha_{rms} = a_{rms}/r = 1606\ rad/s^2$. The required torque can then be calculated from the formula:

$$T = (J_m + 1/\eta\, m\, r^2)\, \alpha$$

This gives the result of $T_{rms} = 0.23\ Nm$ which is less than $0.30\ Nm$ specifications for the given motor at the given angular velocity. This simple calculation does not intend to estimate precisely the values to be achieved, but rather serves as an indicator of the feasibility of the device.

C. 4. 2. Joints

The end of links should be connected to actuators and platform using universal joints. Universal joints (Hooke, U-joints, gimbals) give a much greater range of motion than ball-and-socket joints [Fitcher86]. That requires additional cylindrical joint in the link to achieve the required five degrees of freedom per link. For the manipulator parameters calculated before, simulation showed that the ball-and-socket joints at the platform should have a workspace of a 155° cone, and those at the base should span a cone of 50°, values that are usually not associated with this type of joints. Double U-joints, as shown in [Fitcher86], are used to make platform ends of two links coincident. That means the

geometry of the platform will be triangular rather than hexagonal, which is a more accurate manipulator configuration.

The CAD model of the Stewart Platform with Fixed Actuators prototype is shown on the image to the left. The stepper motors are coupled to racks and pinions elevating the U-joints at the lower end of the links. The U-joints are represented by spheres for simplicity. The upper ends of three pairs of links are connected to a double, single-sided U-joint. The manipulator will eventually be used in the upside-down position.

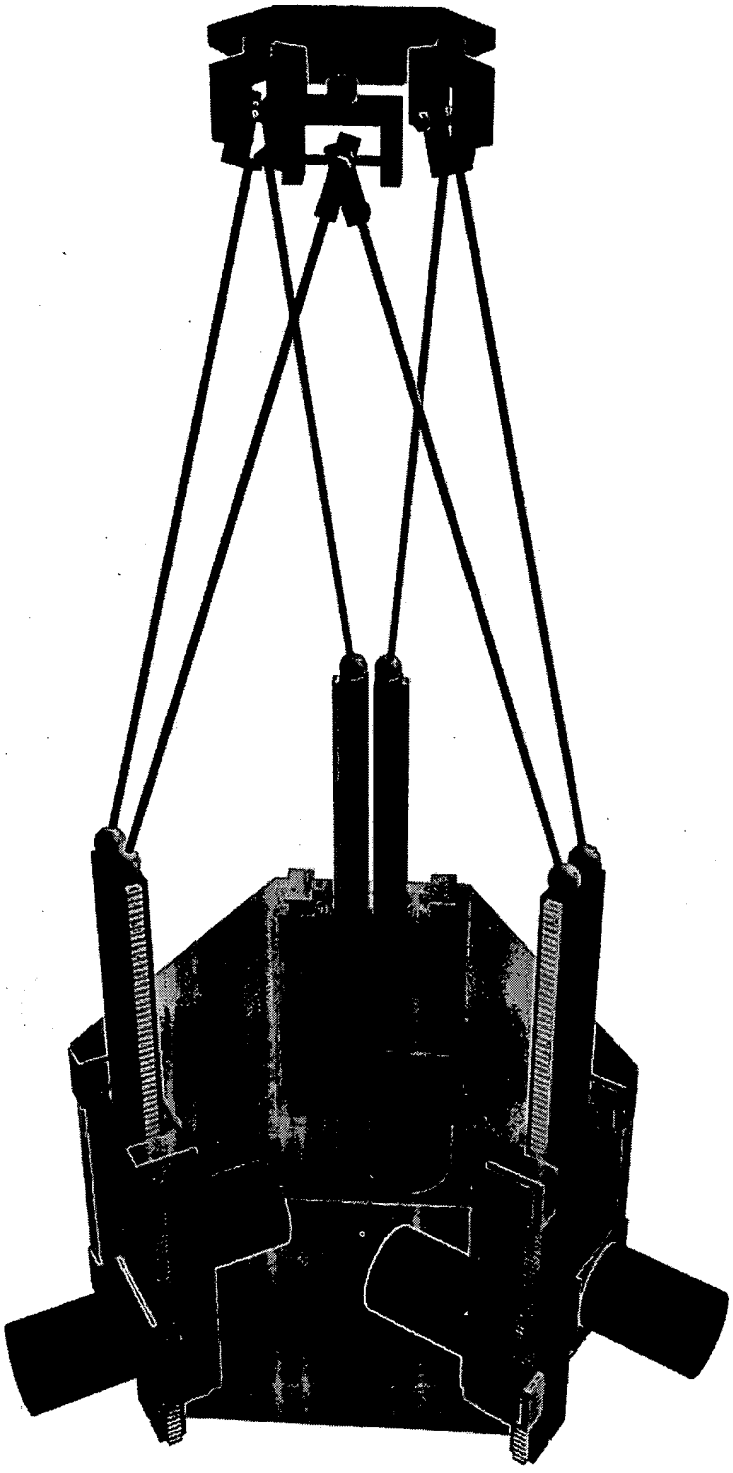

Figure 10. The CAD model of the Stewart Platform with Fixed Actuators, using the dimensions calculated in this paper (CAD design by Joshua Targownik).

D. VISION, CONTROL AND TOOLING SUBSYSTEMS

This thesis is concerned with the mechanical aspect of building a CABG surgery platform. However, we will briefly discuss the necessary requirements for vision, control and tool subsystems needed for the actual working device.

The task of the Stewart Platform manipulator is to carry the camera and the motorized surgical instruments maintaining a constant pose with respect to the heart. That can be achieved by controlling the manipulator closed loop, by means of vision and control subsystems. The vision subsystem provides the relative position of the heart relative to the actuated platform. The control subsystem takes that data and calculates the next position of the platform. This feedback from the vision subsystem should be generated in real-time and contain 6-DOF positioning information. The choice of the vision sensors depends on the required accuracy and system bandwidth.

Since the surgeon can operate using the input from monocular or stereoscopic images that are stabilized, the same images can be used for the feedback. The problem of maintaining the constant pose is then expressed in terms of vision data, and it is called image based servoing. This method operates in the following way. The first image of the tracked object is taken and a reference feature vector is defined from this image. The feature vectors are then calculated from all subsequent images of the moving object. The difference between the reference and the new feature vectors defines the error vector. From the error vector, the controller derives the position error and generates appropriate trajectory. To enhance the visual tracking accuracy and speed, special markers are usually placed on the tracked object, which can be imaged robustly. The markers can be color coded [Wei97] to allow fast computation of position and orientation of the heart. The number of markers should be redundant in case that some of them are occluded by the surgical instruments or bleeding from the surrounding tissue.

The bandwidth of the system has to be sufficient to follow the motion of the heart. That means that the manipulator has to be faster than the beating heart and that the sampling rate of the vision system needs to be high. The faster alternative to the off-the-shelf video cameras is the microsonometry system. They are small sonic transducers that can be placed on the surface of the heart and on the platform. For example, ultrasonic spatial localization device Sonic Digitizer GP8-3D (Science Accessories Corp., Stratford, Conn.) could determine the positions of ultrasound transmitters in space, sampling the distances between the transmitters at the rate of 24kHz [Reinhardt96].

The control subsystem has the task of generating the trajectory of the Stewart Platform manipulator. The heart motion is fast and the delays of the platform and the vision subsystem have to be eliminated. The real-time coordination of a robotic manipulator with a moving target is described in [Allen93]. The tracking is performed there using optical flow and predictive Kalman filtering to null out video processing delays. The motion of the heart is approximately repetitive and periodic. That makes the repetitive control laws well suited for this problem. The repetitive and learning controllers use the information from the previous periods to calculate the trajectory in the future. For example, a simple learning control algorithm could be used [Phan88]:

$$u_{k+1}(t) = u_k(t) + \Phi e_k(t)$$

The command signal $u_{k+1}(t)$, in the $(k+1)$-th repetition is adjusted proportional to the error $e_k(t)$ in the k-th repetition, Φ is a gain matrix. Using learning control, periodic motion of the heart can be tracked with zero time lag [Arimo93], which is not possible to achieve using causal filters. The start of each repetition can be accurately determined from the heart ECG signal or from the external source (pacemaker) if the heart is paced.

With respect to tooling, different types of telerobotic surgical instruments have been implemented. Our device requires custom made telerobotic end-effectors that will be small, rigid and lightweight. The instruments need to be small and rigid to minimize

oscillations due to the movement of the platform. Cable driven tools, as described in [Schener95] would not therefore be appropriate, and magnetically levitated master-slave surgical instruments [Salcu97] are too massive. An interesting design of closed link master-slave surgical manipulator is described in [Mitsu97]. This manipulator is driven directly by an electromotor. For the CABG surgery device, a similar design can be employed, but the motors should be positioned off the platform in order to decrease the instrument weight.

E. CONCLUSION

The Stewart Platform-type manipulator has been described as a platform for a CABG surgery device on a beating heart. Manual surgery on a beating heart represents a major difficulty for surgeons if the heart is not restrained. A robotic device would help the surgeon perform this operation by maintaining a constant pose between the telerobotic instruments and a target on the heart surface. The Stewart Platform-type manipulator has better precision and stiffness, and smaller overall dimensions than equivalent conventional serial-link manipulators. Its small workspace is large enough to carry out surgery. The simplicity of its inverse kinematics makes it well suited for real time trajectory calculation with a high update rate. A modified version of this type of manipulator, called Stewart Platform with Fixed Actuators (SPFA), appears to be a more appropriate option for high-speed operation with small overall dimensions. This paper gives equations for the inverse kinematics and a procedure for obtaining forward kinematics. The dimensions of the manipulator are determined by minimizing the overall size while keeping the structure away from the singular positions. The sensitivity of the platform pose is analyzed as a function of the actuator step size and the platform and base shape. Simulations have shown that the calculated dimensions are valid for the required workspace. Finally, practical aspects of building such a device are considered and it is shown that required motion can be achieved using readily available actuators.

F. LITERATURE

[Allen93] Allen P, Timcenko A, Yoshimi B, Michelman P: **Automated Tracking and Grasping of a Moving Object with a Robotic Hand-Eye System.** *IEEE Transactions on Robotics and Automation*, April 1993, 152-165.

[Alusi97] G Alusi, AC Tan, AD Linney, K Raoof, A Wright: **Three Dimensional Tracking with Ultrasound for Augmented Reality Applications in Skull Base Surgery**, *CVRMed-MRCAS'97 Proceedings,* 1997, 511-517

[April96] EW April: **Clinical Anatomy**, Williams & Wilkins, 1996

[Arimo93] **Learning Control.** S Arimoto, *Robot control : dynamics, motion planning, and analysis.* Ed. Spong, IEEE Press 1993

[Borst97] C Borst, WP Santamore, NG Smedira, JJ Bredee: **Minimally Invasive Coronary Artery Bypass Grafting: On the Beating Heart and via Limited Access.** *Ann Thorac Surg* 1997;63:S1-5

[Brandt97] G Brandt, K Radermacher, S Lavallee, H-W Staudte, G Rau: **A Compact Robot for Image Guided Orthopedic Surgery**, *CVRMed-MRCAS'97 Proceedings,* 1997, 767-778

[Burdea96] GC Burdea: **General-Purpose Robotic Manipulators: A Short Survey.** *Computer Integrated Surgery.* Ed. Taylor, MIT Press, 1996, 257-262

[CIS96] **Computer Integrated Surgery** edited by RH Taylor, S Lavallee, GC Burdea, R Mosges, MIT Press, 1996

[Cremer97] J Cremer, M Struber, T Wittwer, A Ruhparwar, W Harringer, J Zuk, D Mehler, A Haverich: **Off-Bypass Coronary Artery Bypass Grafting via Minithoracotomy Using Mechanical Epicardial Stabilization.** *Ann Thorac Surg* 1997 Jun; 63 (6 Suppl):S79-S83

[Cutting96] CB Cutting, FL Bookstein, RH Taylor: **Applications of Simulation, Morphometrics, and Robotics in Craniofacial Surgery.** *Computer Integrated Surgery.* Ed. Taylor, MIT Press, 1996, 641-662

[CVRMed95] **First International Conference, CVRMed'95 - Proceedings**. Edited by Nicholas Ayache, Springer-Verlag 1995

[CVRMed97] **CVRMed-MRCAS'97 First Joint Conference Computer Vision, Virtual Reality and Robotics in Medicine and Medical Robotics and Computer-Assisted Surgery**, 1997, Proceedings

[Dickstein96] ML Dickstein, K Todaka, D Burkhoff. **3-D Modeling of the Right Ventricle Using Sonometrics Digital Sonomicrometry System.** *Validation study in progress.*

[Fitcher86] EF Fitcher: A Stewart Platform-Based Manipulator: **General Theory and Practical Construction**. *The International Journal of Robotic Research*, Vol 5 No 2, Summer 1986, 157-182

[Grace93] KW Grace, JE Colgate, MR Glucksberg, JH Chun: **A Six Degree of Freedom Micromanipulator for Ophtalmic Surgery**. *1993 IEEE International Conference on Robotics and Automation*, Vol. 1, 630-635

[IEEE96] **IEEE engineering in Medicine and Biology Magazine**, Vol. 15, No. 2, March/April 1996

[Khoda96] K Khodabandehloo, PN Brett, RO Buckingham: **Special Purpose Actuators and Architectures for Surgical Robots.** *Computer Integrated Surgery.* Ed. Taylor, MIT Press, 1996, 263-276

[Lavallee96] S Lavallee, J Troccaz, L Gaborit, P Cinquin, AL Benabid, D Hoffmann: **Image-Guided Operating Robot: A Clinical Application in Stereotactic Surgery.** *Computer Integrated Surgery.* Ed. Taylor, MIT Press, 1996, 343-352

[Mack97a] M Mack, TE Acuff, H Casimir-Ahn, UJ Lonn, EW Jansen: **Video-Assisted Coronary Artery Bypass Grafting on a Beating Heart**. *Ann Thorac Surg* 1997 Jun; 63 (6 suppl):S79-S83

[Mack97b] M Mack, T Acuff, P Yong, GK Jett, D Carter: **Minimally Invasive Thoracoscopically Assisted Coronary Artery Bypass Surgery**. *Eur J Cardiothorac Surg* 1997 Jul;12(1):20-24

[McAcree96] PR McAcree, RW Daniel: **A Fast, Robust Solution to the Stewart Platform Forward Kinematics**. *Journal of Robotic Systems* 13(7), 407-427 (1996)

[Merletwww] J-P Merlet: **Parallel Manipulators: State of the Art and Perspectives.** *http://www.inria.fr/prisme/personnel/merlet/Etat/etat_de_lart.html*

[Mishra97] YK Mishra, Y Mehta, Juneja R, RR Kasliwal, S Mittal, N Trehan: **Mammary-Coronary Artery Anastamosis Without Cardiopulmonary Bypass Through a Minithoracotomy**. *Ann Thorac Surg* 1997 Jun; 63 (6 Suppl):S114-S118

[Mitsu97] M Mitsuishi, H Watanabe, H Nakanishi, H Kubota, Y Iszuka: **Dexterity Enhancement for a Tele-micro surgeru System with Multiple Macro-micro Co-located Operation Points Manipulators and Understanding of the Operator's Intention** , *CVRMed-MRCAS'97 Proceedings,* 1997, 821-830

[Nguyen93] CC Nguyen, SS Antrazi, Z-L Zhou, CE Campbell Jr: **Adaptive Control of a Stewart Platform-Based Manipulator**. *Journal of Robotic Systems* 10(5), 657-687 (1993)

[Peria95] O Peria, L Chavalier, A Francois-Joubert, J-P Caravel, S Dalsoglio, S Lavallee, P Cinquin: **Using a 3D Position Sensor for Registration of SPECT and US Images of the Kidney** *First International Conference, CVRMed'95 - Proceedings.* Ed. Ayache, 1995, 23-29

[Pichler97] CV Pichler, K Radermacher, W Boeckmann, G Jakse, G Rau: **3D-Visualisation for Image Guided Surgery - A Case Study in Video Endoscopy**. , *CVRMed-MRCAS'97 Proceedings,* 1997, 311-314

[Reinhardt96] HF Reinhardt: **Neuronavigation: A Ten-Year Review.** *Computer Integrated Surgery.* Ed. Taylor, MIT Press, 1996, 329-342

[ROB93] **Robot control : dynamics, motion planning, and analysis**. Edited by Mark W. Spong, F.L. Lewis, C.T. Abdallah, IEEE Press 1993

[Rovetta96] A Rovetta, R Sala, F Cosmi, X Wen, S Milanesi, D Sabbadini, A Togno, L Angelini, AK Bejczy: A New Telerobotic Application: **Remote Laparoscopic Surgery Using Satelites and Optical Fiber Networks for Data Exchange.** *The International Journal of Robotics Research*, Vol. 15, no. 3, June 1996, 267-279

[Salcu97] SE Salcudean, S Ku, G Bell: **Performance Measurement in Scaled Teleoperation for Microsurgery** , *CVRMed-MRCAS'97 Proceedings,* 1997, 789-798

[Santos95] JJ Santos-Mune, MA Peshkin, S Mirkovic, SD Stulberg, TC Kienzle: **A Stereotactic/Robotic System for Pedicle Screw placement**. *Proceedings of Medicine Meets Virtual Reality III*, January 1995, p.326-333

[Schenker95] PS Schenker, H Das, TR Ohm**: A New Robot for High Dexterity Microsurgery** *First International Conference, CVRMed'95 - Proceedings.* Ed. Ayache, 1995, 115-122

[Taylor94] RH Taylor, BD Mittelstadt, HA Paul, W Henson, P Kazanzides, JF Zuhars, B Williamson, BL Mustis, E Glassman, WL Bargar: **An Image-Directed Robotic System for Precise Orthopaedic Surgery**. *IEEE Transactions on Robotics and Automation, vol. 10, no. 3, June 1994*

[Taylor96] RH Taylor, J Funda, B Eldridge, D LaRose, S Gomory, K Gruben, M Talamini, L Kavoussi, J Anderson**: A Telerobotic Assistant for Laparoscopic Surgery**. *Computer Integrated Surgery.* Ed. Taylor, MIT Press, 1996, 581-592

[Treas97] Treasure T: **Minimal access surgery**. *Heart* 77(4), 304-306 (1997)

[Treat97] Treat M, personal communication (1997)

[Troccaz97] J Troccaz, M Peshkin, B Davies**: The Use of Localizers, Robots and Synergistic Devices in CAS** , *CVRMed-MRCAS'97 Proceedings,* 1997, 727-736

[Uenoh95] M Uenohara, T Kanade: **Vision-Based Object Registration for Real-Time Image Overlay**, *First International Conference, CVRMed'95 - Proceedings.* Ed. Ayache, 1995, 13-22

[Wei97] G-Q Wei, Klaus Arbter, G Hirzinger: **Automatic Tracking of Laparoscopic Instruments by Color Coding** , *CVRMed-MRCAS'97 Proceedings,* 1997, 357-367

[Yang84] DCH Yang, TW Lee: **Feasibility Study of a Platform Type of Robotic Manipulators from a Kinematic Viewpoint**. *Journal of Mechanisms, Transmissions, and Automation in Design*, June 1984, Vol 106, 191-198

[Yosh95] Yoshimi B, Allen P: **Active Uncalibrated Visual Servoing**. *IEEE Transactions on Robotics and Automation*. V. 11, N. 5, August 1995, 516-521

G. Acknowledgments

Peter Allen, Michael Treat, Marc Dickstein

This Page is Inserted by IFW Indexing and Scanning Operations and is not part of the Official Record

BEST AVAILABLE IMAGES

Defective images within this document are accurate representations of the original documents submitted by the applicant.

Defects in the images include but are not limited to the items checked:

- ☑ BLACK BORDERS
- ☐ IMAGE CUT OFF AT TOP, BOTTOM OR SIDES
- ☐ FADED TEXT OR DRAWING
- ☐ BLURRED OR ILLEGIBLE TEXT OR DRAWING
- ☐ SKEWED/SLANTED IMAGES
- ☐ COLOR OR BLACK AND WHITE PHOTOGRAPHS
- ☐ GRAY SCALE DOCUMENTS
- ☐ LINES OR MARKS ON ORIGINAL DOCUMENT
- ☐ REFERENCE(S) OR EXHIBIT(S) SUBMITTED ARE POOR QUALITY
- ☐ OTHER: _____

IMAGES ARE BEST AVAILABLE COPY.
As rescanning these documents will not correct the image problems checked, please do not report these problems to the IFW Image Problem Mailbox.